Second International Symposium on Marine Propulsors
smp'11, Hamburg, Germany, June 2011
Workshop: Cavitation on foil

RANS Simulation of the Delft Twist 11 Foil

Thierry Maquil, Bahaddin Cankurt, Patrick Schiller, Sergey Yakubov, Moustafa Abdel-Maksoud, Thomas Rung

Institute for Fluiddynamics and Shiptheory, Hamburg University of Technology (TUHH), Hamburg, Germany

ABSTRACT

The paper reports the results of cavitation simulations of the Delft-Twist-11 hydrofoil. The simulations are performed using a URANS approach with a $k-\omega$ turbulence model. Cavitation is modelled by a VOF-based Euler-Euler approach using the Zwart model to approximate the mass transfer between the liquid phase and the vapout phase. Results show a fair level of predicitive agreement with experimental observations.

Keywords

CFD, cavitation model, Euler-Euler, VOF, Delft twist 11 hydrofoil

1 INTRODUCTION

The paper is concerned with cavitation simulations of the Delft-Twist-11 foil. The configuration has been analysed experimentally by Foeth (2008) in a cavitation tunnel. A particular feature of the symmetric geometry is the variable angle of attack in span-wise direction. Accordingly, the relative angle increases by 11° towards the centre.

Various steady and forced unsteady approach-flow conditions have been measured. The present study is confined to steady flows at Reynolds number $Re = 1.5 \cdot 10^6$ and cavitation number $\sigma = 1.07$. Notice that the experimental setup reports two guidance foils located upstream of the investigated hydrofoil, which can induce an unsteady approach flow using moveable flaps. The presently meshed configuration considers these two non-oscillating guidance foils upstream the twisted Delft foil.

The cavitating flow displays a three-dimensional and periodic behaviour. Different types of cavitation and a re-entrance jet can be observed. Thus, contrary to the usually computed two-dimensional validation cases (e.g. NACA66mod), the case offers more complex hydrodynamics and is a prime validation candidate when heading for more complex applications.

2 NUMERICAL METHOD

FreSCo^+ FreSCo^+ is a spin-off of FreSCo, a joint development of Hamburg University of Technology (TUHH), Hamburgische Schiffbau-Versuchsanstalt (HSVA) and Maritime Research Institute Netherlands (MARIN). The original code was developed within the scope of the EU initiative VIRTUE. The procedure uses a segregated algorithm based on the strong conservation form of the momentum equations. It employs a cell-centred, co-located storage arrangement for all transport properties. Structured and unstructured grids, based on arbitrary polyhedral cells or hanging nodes, can be used.

The implicit numerical approximation is second-order accurate in space and time. Integrals are approximated using the conventional mid-point rule. The solution is iterated to convergence using a pressure-correction scheme. Various turbulence-closure models are available with respect to statistical (RANS) or scale-resolving (LES, DES) approaches.

Two-phase flows are addressed by interface-capturing methods based upon the Level-Set or Volume-of-Fluid (VOF) technique. Since the data structure is generally unstructured, suitable pre-conditioned iterative sparse-matrix solvers for symmetric and non-symmetric systems (e.g. GMRES, BiCG, QMR, CGS or BiCGStab) can be employed. The algorithm is parallelised using a domain-decomposition technique based on a Single Program Multiple Data (SPMD) message-passing model, i.e. each process runs the same program on its own subset of data. Inter-processor communication employs the MPI communications protocol. Load balancing is achieved using the ParMETIS partitioning software.

Cavitation is modelled using either mass-transfer models (Euler-Euler) or two-way coupled Euler-Lagrange approaches.

Cavitation Model An extended VOF method is used to model the cavitation. The fluid is considered to be a mixture between water (l) and vapour (v). Optionally a non-condensable gas fraction can be considered (Singhal et al., 2002). The properties of the mixture are computed from the volume fraction of the phases, i.e. the vapour-volume fraction is defined by

$$\alpha = \frac{V_\mathrm{v}}{V_\mathrm{l} + V_\mathrm{v}} \, . \tag{1}$$

Exemplary the density of the fluid yields

$$\rho = \rho_\mathrm{v} \, \alpha_\mathrm{v} + \rho_\mathrm{l} \, (1 - \alpha) \, . \tag{2}$$

A transport equation for the vapour-volume fraction is solved

$$\frac{\partial \alpha}{\partial t} + \frac{\partial \alpha \, u_i}{\partial x_i} = s_\mathrm{cav} \, , \tag{3}$$

whereby s_{cav} is a source term describing the volume transfer between the liquid and the vapour phase. The source term can be approximated via several models, in the present work it is obtained from the Zwart-model (Zwart et al., 2004)

$$s_{\text{cav}} = \begin{cases} F_{\text{vap}} \cdot \frac{3\ \alpha_{\text{nuc}}\ (1-\alpha)}{R_0} \cdot \dot{R} & \text{(vapourization)} \\ F_{\text{cond}} \cdot \frac{3\ \alpha}{R_0} \cdot \dot{R} & \text{(condensation)} \end{cases} . \quad (4)$$

The Zwart-model inheres two empirical constants F_{vap} and F_{cond} which allow to distinguish between vaporisation and condensation. The nucleation site volume fraction α_{nuc} and the corresponding nucleation site radius R_0 are two additional *water-quality* parameters. The bubble radius change $\dot{R}$ is normally defined via a simplified Rayleigh-Plesset (R.-P.) equation which only depends on the pressure difference between the ambient and saturation pressures. Brennen (2005) proposes an alternative derivation of the bubble radius change which considers all terms of the R.-P. equation

$$\begin{aligned} \dot{R}^2 \quad = \quad & \frac{p_{\text{sat}} - p}{3/2\ \rho_{\text{l}}} \cdot \left[1 - \left(\frac{R_0}{R} \right)^3 \right] \\ & + \frac{2\ p_{\text{G}_0}}{\rho_{\text{l}}} \cdot \left(\frac{R_0}{R} \right)^3 \cdot \ln \left(\frac{R}{R_0} \right) \\ & - \left(\frac{2\ \sigma_0}{\rho_{\text{l}} R} + \frac{4\ \mu_{\text{l}} \dot{R}}{\rho_{\text{l}} R} \right) \cdot \left[1 - \left(\frac{R_0}{R} \right)^2 \right] , \quad (5) \end{aligned}$$

whereby ρ_{l} and ν_{l} denotes the liquid density and viscosity, σ_0 is the surface tension, p_{G_0} the initial partial gas pressure, R the actual bubble radius and R_0 the initial bubble radius, respectively. The influence of the turbulence on the cavitation is considered via an increase of the saturation pressure due to turbulence energy $p_{\text{sat}} = p_{sat} + 0.195\ \rho\ k$ (Singhal et al., 2002).

The SIMPLE method described by Sauer (2000) is used for the coupling between momentum and pressure equations.

The model tends to initiate vapour-volume fraction outside the physical bounds ($\alpha \in [0, 1]$), the easiest method to handle this issue is to limit the vapour-volume fraction to the admissible bounds. Alternatively, the source term is manipulated in order to drive the vapour-volume fraction back into its bounds. The sign of the source term depends on the sign of the pressure difference.

Additionally, the source term is limited in accordance with the possible rate of change.

3 SIMULATION SETTINGS

Foil Geometry The present work deals with a simulation of experimental study of the Delft foil performed by (Foeth, 2008). The span of the foil is 300 mm and the chord length is $c = 150$ mm. The section shape of the foil is uniform (symmetrical NACA 4-digit NACA0009) over the whole span, but the angle of attack (AOA) varies in span-wise direction (a relative change of 11 ° from the end of the wing to mid-span). To reduce the optical blocking of the mid-section plane the sections rotate around $x/c = 0.75$. On the wall the angle of attack is set to $-2°$. Upstream the investigated foil two NACA 63 A010 foils are located to mimic unsteady approach flows. In the present work these guidance foils do not move.

Coordinate System A standard right-hand coordinate system with the x-axis in flow direction, the y-axis in span-wise direction and the z-axis directed upwards is used as reference coordinate system. The origin of the system is at mid-chord at mid-height of the wing section on the tunnel wall.

Computational Domain The computational domain extensions are given in the workshop description. The length is chosen as 7 chord lengths, starting 2 chord lengths ahead of the leading edge and ending 4 chord lengths behind the trailing edge. The height of the domain is chosen as 2 chord lengths corresponding to the height of the test section. In span-wise direction only half of the wing is calculated, i.e. a symmetry boundary condition is used at the centre of tunnel. In Figure 1 the computational domain and the Delft foil are sketched.

Grid The grid is generated in *ICEM CFD*. A C-grid with H-grids ahead and behind the foils (Delft foil and oscillating foils) are used for the blocking structure. Figure 1 represent the scenario. The resolution of the grid is chosen with 100 cells around the Delft foil in longitudinal direction with a refinement at the leading edge. In span-wise direction the domain is equally divided into 30 parts. Low Reynolds ($Y^+ < 1$) boundary layer is applied around the Delft foil. The grid properties are summarised in Table 1.

Table 1: Grid Quality.

Cells	300000
Determinant	> 0.7
Angle	$> 45°$
Quality	> 0.7

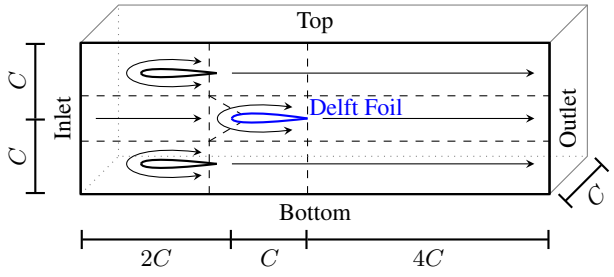

Figure 1: Blocking structure and computational domain.

Global Settings First, a simulation without cavitation is run to generate a restart file for the cavitating simulation. The non-cavitating simulations are performed as steady simulations. Pressure, momentum and turbulence equations are solved. The turbulence is modelled with the k-ω

standard model. The QUICK convection scheme without limitations is used for all properties.

For the cavitating simulation an unsteady simulation with the Zwart cavitation model is performed. The time step is set to $\Delta t = 1.\ 10^{-5}$ s. The resulting Courant number falls below $Co < 1$. In the test case description no information about the water quality and bubble size/concentration is given. The empirical Zwart coefficients are set to the values reported by (Zwart et al., 2004) ($F_{\text{vap}} = 50.0$, $F_{\text{cond}} = 0.01$, $\alpha_{\text{nuc}} = 1.\ 10^{-6}$ and $R_0 = 5.\ 10^{-4}$ m). The initial bubble radius is set to $R_0 = 1.\ 10^{-6}$ m.

Boundary Conditions At the inlet a uniform velocity profile is applied. The velocity is 6.97 m/s corresponding to a Reynolds number $Re = 1.5 \cdot 10^6$. At the outlet a pressure boundary condition is applied. The outlet pressure is set to 29 kPa. The saturation pressure is $p_{\text{sat}} = 2970$ Pa yielding a cavitation number $\sigma = 1.07$. The tunnel walls and the guidance foils are simplified as slip walls. On the centre plane a symmetry boundary condition is used. A *Universal High Reynolds* wall function model is applied on the Delft foil.

4 RESULTS

Total vapour-volume fraction The periodicity of the cavitating flow is analysed through the total vapour-volume fraction c_{tot}. This ratio is the difference between the total vapour-volume and the total volume

$$\alpha_{\text{tot}} = \frac{\sum_{\text{CVs}} \alpha\, V}{\sum_{\text{CVs}} V}, \tag{6}$$

with V the volume of a control volume (CV). Figure 2 shows the temporal evolution of the total vapour-volume fraction. The first seven periods are of initial transient behaviour. The amplitude is twice as high as at the converged state. The shedding frequency is determined with a Fast Fourier transform of the last 11 periods. The frequency yields $f = 38.79$ Hz, corresponding to a period of $T = 0.026$ s. The blue squares in figure 2 highlight the time-snapshots which are used in the subsequent evaluation.

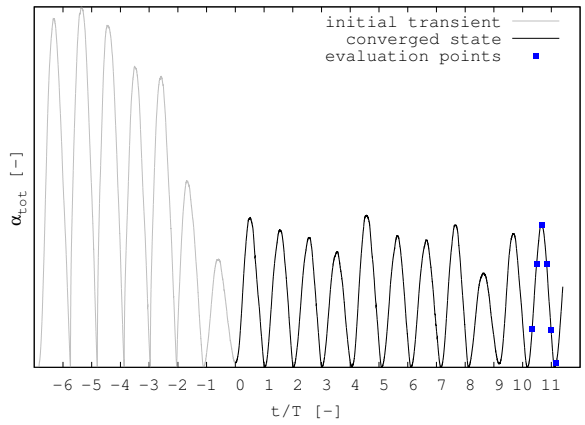

Figure 2: Total vapour-volume fraction

Convergence In line with the total vapour-volume fraction, the convergence of the cavitating simulation shows a strong periodic behaviour. The residuals of the momentum, pressure and turbulence equations at the first outer iteration are below $1.\ 10^{-8}$, $4.\ 10^{-7}$ and $2.\ 10^{-4}$, respectively. The residual of the cavitation equation, on the other hand, varies between 0.1 and $2.\ 10^{-4}$. The highest residual occurs at the collapse of the cavitation region.

Cavitation region Figure 3 shows a sequence of 6 images over one shedding period viewed from the top of the Delft foil. The normalised pressure distribution on the foil c_p is plotted, the cavitation region is illustrated with a white contour at iso-surface $\alpha = 0.5$. Additionally to the snapshots, videos of the cavitation behaviour from different view points are available.

Pressure distribution Figure 4 and 5 show the normalised pressure distribution at different span-wise planes for the non-cavitating and the cavitating cases. A sketch of the span-wise planes (y/C =0.1, 0.2, 0.3, 0.4 and 0.5) is given at the bottom of figure 4.

For the non-cavitating case experimental data of the VIRTUE workshop is available, the simulation and the experiment are in good agreement.

The non-cavitating case is summarised with 6 snapshots over a period where only 3 planes (y/C =0.1, 0.3 and 0.5) are considered. The location of the cavitation region is given by the pressure plateau at $c_p = 1.07$ which corresponds to the predefined cavitation number of the test case. Additionally, the temporal change of the cavitation region can be distinguished by the temporal variation in the pressure distribution.

Dimensionless forces The dimensionless lift c_{L} and drag c_{D} coefficients are defined as

$$c_{\text{L}} = \frac{L}{0.5\ \rho_{\text{l}}\ v_\infty^2\ A} \quad \text{and} \quad c_{\text{D}} = \frac{D}{0.5\ \rho_{\text{l}}\ v_\infty^2\ A}, \tag{7}$$

whereby L denotes the lift force and D the drag force acting on the hydrofoil, respectively. As reference surface the projected surface area $A = 2C^2$ is chosen.

The force coefficient of the non-cavitating simulation are summarised in Table 2. Computations with a finer mesh of 800 thousand cells reveal only marginal differences.

Table 2: Lift and drag coefficient non-cavitating case.

	c_{D} [-]	c_{L} [-]
Pressure	0.0156	0.3655
Friction	0.0086	-0.0002
Total	0.0242	0.3653

In figure 6 the temporal evolution of the force coefficients of the cavitating simulation are plotted. The data is not average, but belongs to the period from which the snapshot are presented (11^{th} period).

5 CONCLUSION

Non-cavitating and cavitating simulations of the Delft Twist 11 foil have been performed with the RANS solver FreSCo^{+}. The results show that three-dimensional cavitation flows can be simulated with a URANS approach combined with VOF-based Euler-Euler methods. The three-dimensional and periodic flow behaviour is reproduced by the simulation. However the method uses empirical coefficients which have a substantial influence on the attainable predicitive accuracy. Moreover, the simulation does not consider any water-quality effects. Future work will address these issues.

6 REFERENCES

C.E. Brennen. *Fundamentals of Multiphase Flows*. Cambridge University Press, 2005.

E.-J. Foeth. *The structure of three-dimensional sheet cavitation*. PhD thesis, Delft University of Technology, 2008.

J. Sauer. *Instationär kavitierende Strömungen - Ein neues Modell, basierend auf Front Capturing (VoF) und Blasendynamik*. PhD thesis, UniversitÃd't Karlsruhe, 2000.

A.k. Singhal, M.M. Athavale, H. Li, and Y. Jiang. Mathematical basis and validation of the full cavitation model. *Journal of Fluids Engineering*, 124:617–624, September 2002.

P.J. Zwart, Gerber A.G., and T. Belamri. A two-phase flow model for predicting cavitation dynamics. In *ICMF 2004 International Conference on Multiphase Flow*, number 152, Yokohama, Japan, 2004.

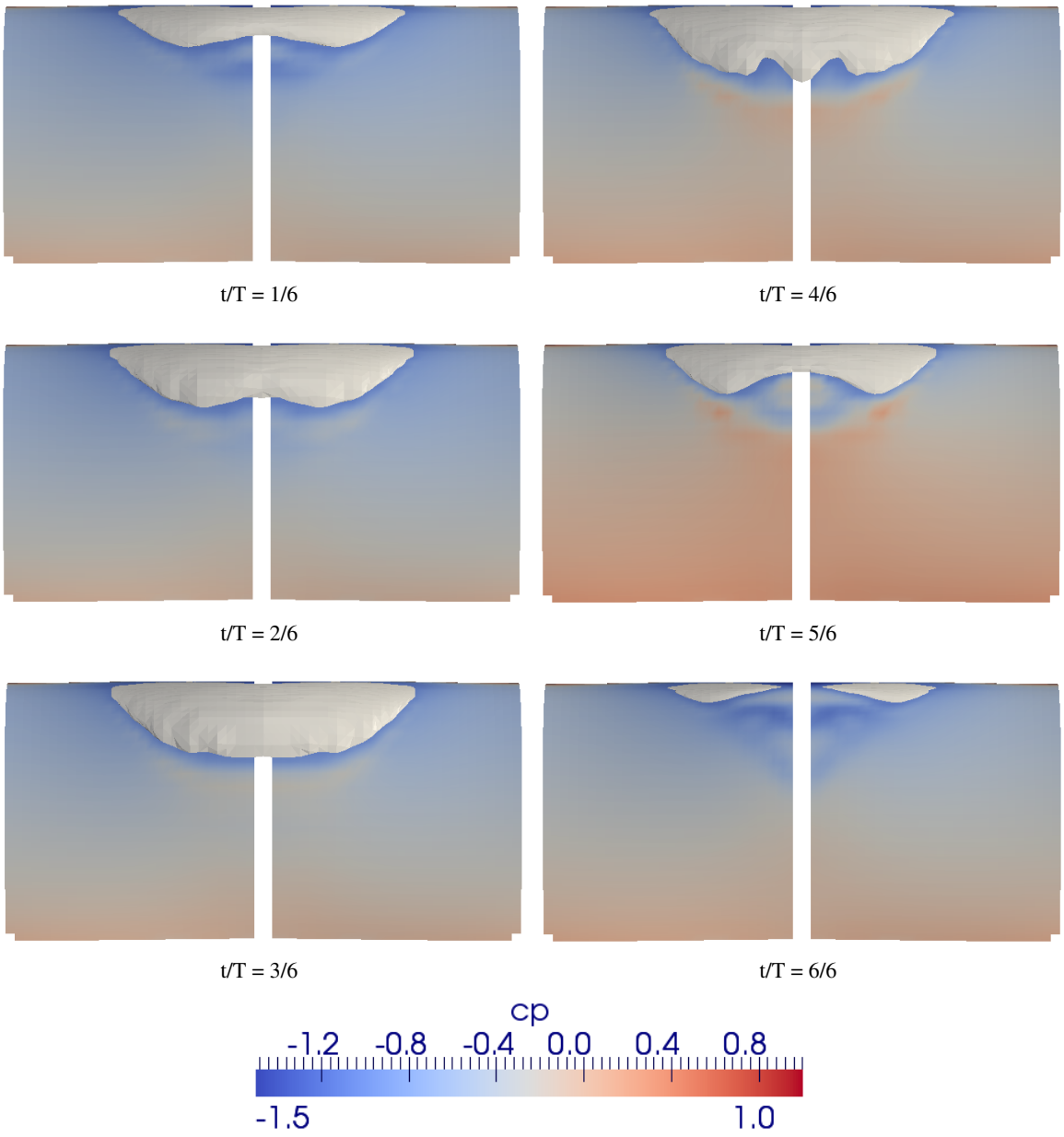

Figure 3: Cavitation extend top view (Iso-surface vapor volume fraction = 0.5).

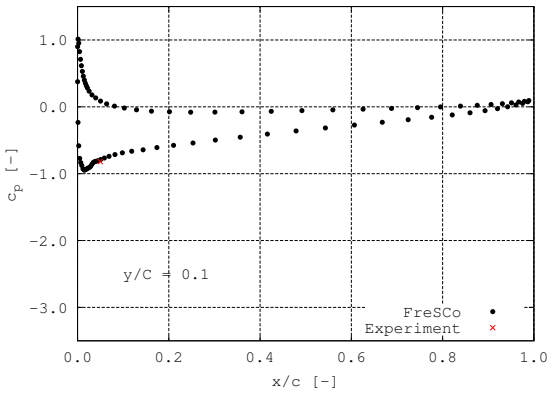

y/C = 0.1

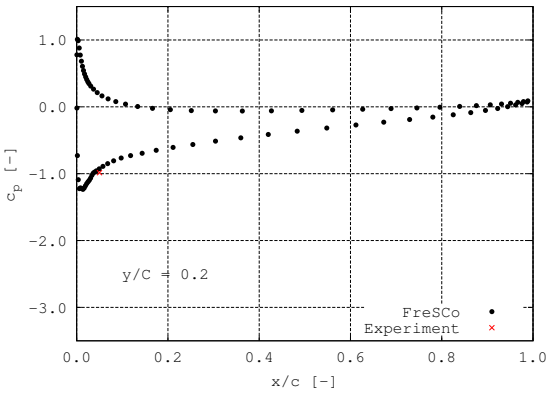

y/C = 0.2

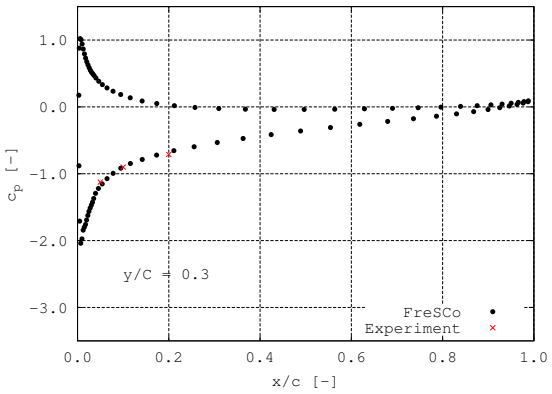

y/C = 0.3

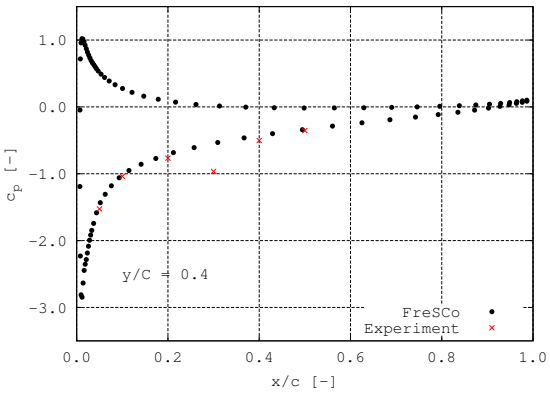

y/C = 0.4

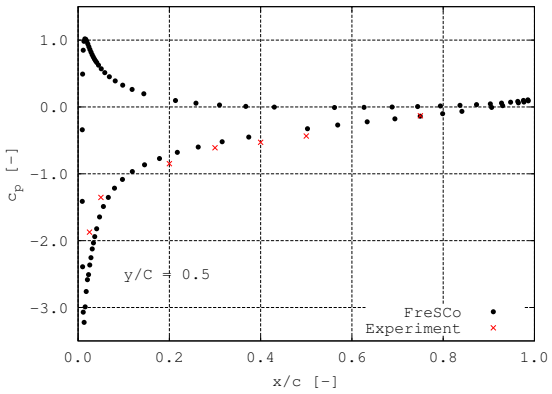

y/C = 0.5

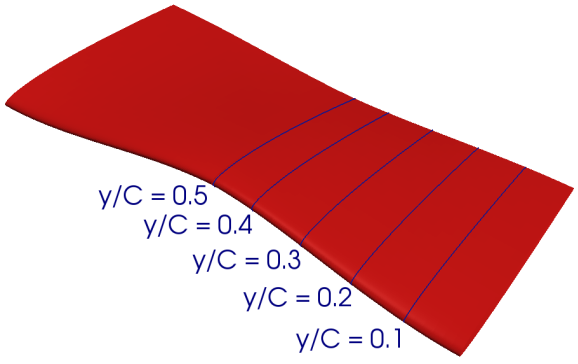

Figure 4: Pressure distribution for non-cavitating simulation.

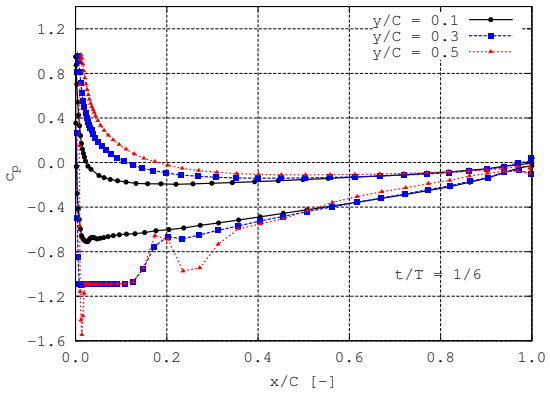

t/T = 1/6

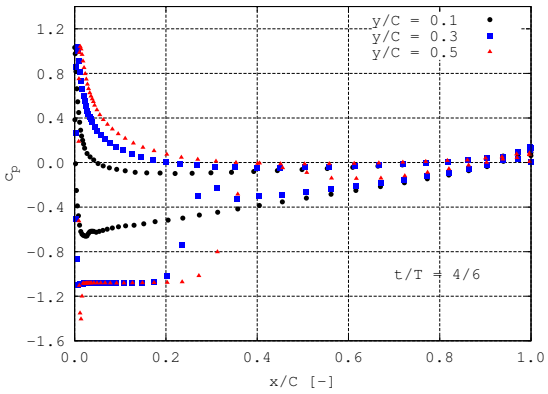

t/T = 4/6

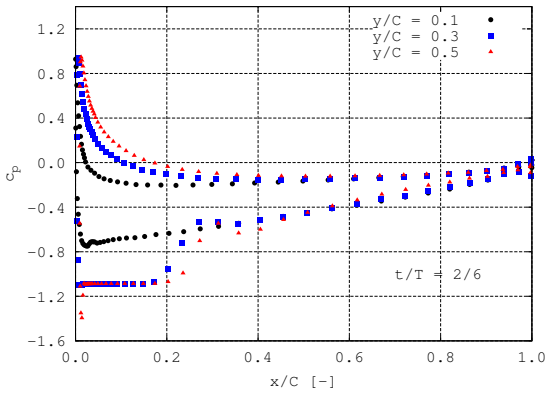

t/T = 2/6

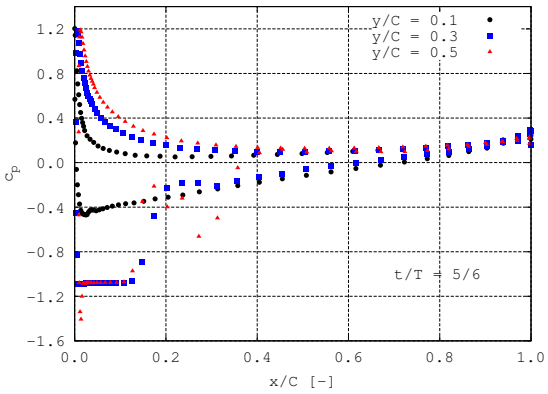

t/T = 5/6

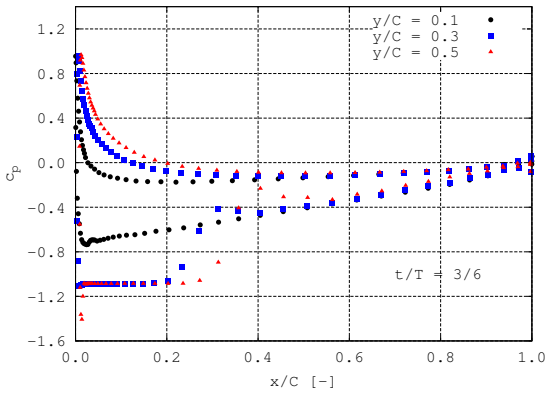

t/T = 3/6

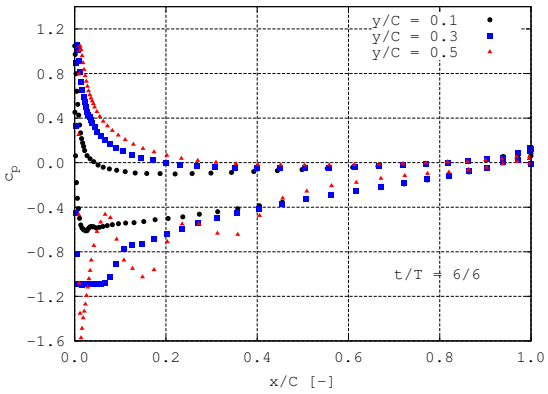

t/T = 6/6

Figure 5: Pressure distribution for cavitating simulation.

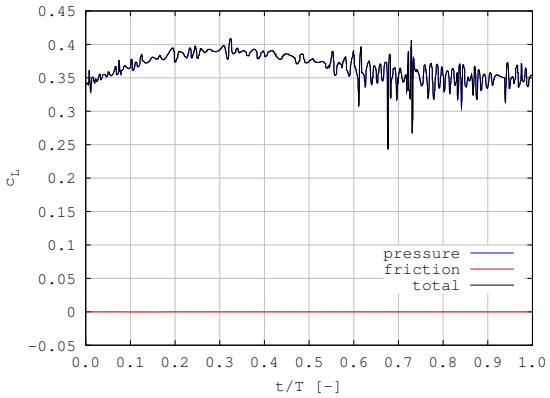

Lift coefficient

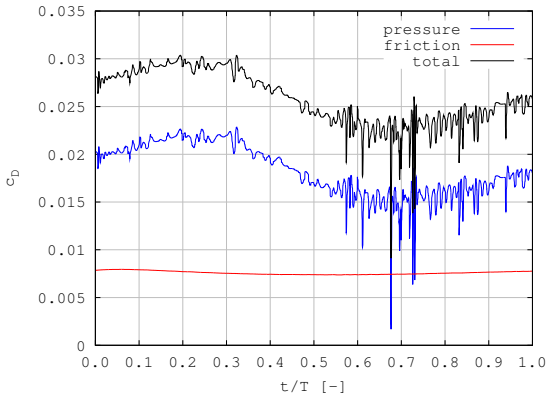

Drag coefficient

Figure 6: Non-dimensional forces for cavitating simulation.